Energy & Environmental Science

ARTICLE

Electronic Supplementary Information (ESI)

Localized anion-rich solvation structure in low-concentration electrolytes enabled by non-coordinating chaotrope for deep-cycling zinc metal batteries

Licheng Miao,‡[a] Guoqiang Ma,‡[b,d] Kaiyue Qiu,[b] Zhiyuan Zhao,[a] Minglu Li,[c] Tongqiang Bi,[b] Kai Yang,[a] Yuanyuan Hu,[a] Yuanyuan Wang,[b] Jing Xu,[a] Lei Ma,*[c] Zhaoxi Shen,*[b] and Ning Zhang*[b,c]

a. College of Chemistry and Material Science, Shandong Agriculture University, Taian 271018, China.

b. College of Chemistry and Materials Science, Hebei University, Baoding 071002, China. E-mail: ningzhang@hbu.edu.cn; zhaoxishen@hbu.edu.cn.

c. Shijiazhuang Shangtai Technology Co., Ltd., Shijiazhuang 050000, China. E-mail: mle617@163.com

d. College of Chemical and Pharmaceutical Engineering, Hebei University of Science and Technology, Shijiazhuang 050018, China

Experimental Section

Preparation of electrolytes and cathodes

Electrolytes: All aqueous electrolytes were prepared using deionized water from the Ultrapure water system. $Zn(CF_3SO_3)_2$ ($Zn(OTf)_2$) (Adamas) was dissolved in deionized water to prepare 1.54 M and 2 M $Zn(OTf)_2$ electrolytes. Electrolytes with varying TM-Urea concentrations were prepared by adding 0.1, 0.3, and 0.5 mL of tetramethylurea (TM-Urea) (Adamas) to 1 mL of a 2 M $Zn(OTf)_2$ electrolyte, yielding formulations denoted as 0.1 TM-Urea, 0.3 TM-Urea, and 0.5 TM-Urea, respectively. The 0.1, 0.3, and 0.5 mL TM-Urea solvents correspond to 0.87, 2.50, and 4.17 mmol, respectively. Given that the Urea and dimethylurea (DM-Urea) are solid powders, we add the same molar weight of Urea and DM-Urea into 1 mL 2 M $Zn(OTf)_2$ to prepare Urea and DM-Urea based electrolytes. For the convenience of comparison, electrolytes by dissolving 2.5 mmol of Urea or DM-Urea in 1 mL of 2 M $Zn(OTf)_2$ solution are denoted as 0.3 Urea and 0.3 DM-Urea, respectively. Additionally, urea/water mixtures were prepared by dissolving 2.5 mmol of each urea-based compound (Urea, DM-Urea, TM-Urea) in deionized water to form H_2O/Urea, H_2O/DM-Urea, and H_2O/TM-Urea solutions. The preparation of electrolyte is easy to scale up by adjusting the volume of the electrolyte and additives.

Cathodes: The $V_2O_5{\cdot}nH_2O$ (VOH) cathode material was synthesized by reacting V_2O_5 powder (Energy Chemical) with H_2O_2 (Aladdin) at room temperature, following methods reported in the literature.[S1,S2] Typically, 0.364 g of V_2O_5 powder was added to 1.6 mL of 30% H_2O_2 in 20 mL of deionized water. The V_2O_5 powder quickly dissolved, forming a deep red solution. After resting for 10 h, the VOH deposits were collected, thoroughly washed with water, and freeze-dried for 12 h. The VOH working electrode was prepared by blending the active material, Super P carbon (Timcal), and polyvinylidene fluoride (PVDF) (Aladdin) in a 7:2:1 weight ratio using N-methyl-2-pyrrolidone (NMP) (Aladdin) as the solvent. The resulting slurry was applied to titanium (Ti) foil (Qingyuan Metal Materials) and dried at 60°C for 10 h under vacuum.

Cell assembling

Coin cells: Zn||Zn symmetric cells were assembled using commercial zinc (Zn) foil (50 µm thickness, 12 mm diameter) (Qingyuan Metal Materials) and Whatman glass microfiber (GF/D) separators (16 mm diameter). Zn||copper (Cu) half-cells were constructed with commercial Cu foil (11 µm thickness, 12 mm diameter) (Qingyuan Metal Materials), Zn foil (50 µm thickness, 12 mm diameter), and GF/D separators (16 mm diameter). Similarly, Zn||Ti half-cells were assembled using commercial Ti foil (20 µm thickness, 12 mm diameter), Zn foil (50 µm thickness, 12 mm diameter), and GF/D separators (16 mm diameter). Zn||VOH full cells were constructed with Zn foil (50 or 20 µm thickness, 12 mm diameter) as the anode, VOH as the cathode (12 mm diameter), and GF/D separators (16 mm diameter). The typical mass loading of the prepared cathode was 2–3 mg cm^{-2} for the coin-type cells. All cells were assembled in CR2032 coin-type casings, with approximately 80 µL of electrolyte added to each cell.

Pouch cells: Each pouch Zn||VOH full cell was composed of a 3 × 3 cm^2 Zn foil (20 μm thickness) as the anode, 3 × 3 cm^2 VOH as the cathode, and a 3 × 3 cm^2 GF/D separator. The pouch cell was sealed in an aluminum (Al)–plastic film (Olegeeino), with 2 mL of electrolyte added. The typical mass loading of the VOH cathode was 26.7 mg cm^{-2} for pouch cells.

Electrochemical tests

Basic electrochemical tests were conducted using a Solartron 1470E electrochemical workstation, while long-term cycling tests were performed on a LANHE CT3002A battery-testing system. The Zn^{2+} plating/stripping Coulombic efficiency (CE) was evaluated using asymmetric Zn||Cu cells, with a cut-off voltage set at 0.5 V. The cycling stability of Zn electrodes was assessed using symmetric Zn||Zn cells. Zn nucleation overpotentials were determined from Zn||Ti asymmetric cells by cyclic voltammetry (CV) in the range of −0.3 to 1.0 V at a scan rate of 1 mV s^{-1}. LSV and Tafel curves were obtained using a three-electrode configuration. For Tafel measurements, Zn served as the working electrode, Ti foil as the counter electrode, and a saturated calomel electrode (SCE) as the reference. Scans were performed from −0.58 to −1.18 V (vs SCE) at a rate of 1 mV s^{-1}. LSV analysis was carried out using Pt foil as both the working and counter electrodes, with SCE as the reference electrode, over a potential range of −0.5 to −2.0 V at a scan rate of 1 mV s^{-1}. Chronoamperometry (CA) tests were performed using Zn||Zn cells under a constant overpotential of −200 mV for 800 s. The electric double-layer (EDL) capacitance was evaluated from CV scans at various rates (10, 12, 14, 16, and 18 mV s^{-1}) over a voltage range of −15 to 15 mV using Zn||Zn symmetric cells. The differential capacitance-potential curve for the Zn||Ti cell was obtained through alternating current (AC) voltammetry at a scan rate of 20 mV s^{-1}, frequency of 50 Hz, amplitude of 5 mV, and phase angles of 0° and 90°, with a voltage range of 0 to 1 V. CV measurements of Zn||VOH full cells were conducted within a potential window of 0.2–1.7 V. EIS measurements were conducted with an amplitude of 5 mV over a frequency range of 100 mHz to 100 kHz. The Zn^{2+} transference number ($t_{Zn^{2+}}$) was calculated using Equation (1):

$$t_{Zn^{2+}} = \frac{I_s(\Delta V - I_0 R_0)}{I_0(\Delta V - I_s R_s)} \quad (1)$$

where I_0 and I_s represent the initial and steady-state currents (μA), respectively, derived from the current–time (*i*–*t*) curve, and R_o and R_s are the interfacial resistances before and after polarization, respectively. A constant potential (Δ*V*) of 20 mV was applied. All symmetric cells were allowed to rest for 5 h prior to measurement. Differential capacitance–potential curves were characterized using phase-selective alternating current (AC) voltammetry in asymmetric Zn||Ti cells. The scans were performed at a rate of 10 mV s^{-1} over a potential range of 0.7 to 0 V vs Zn^{2+}/Zn. The AC frequency was 6 Hz, with a modulation amplitude of 5 mV. Phase angles of 0° and 90° were selected for analysis. The phase shift (*Φ*) was calculated using Equation (2):

$$\Phi = \tan^{-1}\frac{i_{90}}{i_0} \quad (2)$$

where i_0 and i_{90} are the AC currents at phase angles of 0° and 90°, respectively. The impedance (Z) was calculated using Equation (3):

$$Z = \frac{\mathrm{A}}{\sqrt{i_{90}{}^2 + i_0{}^2}} \quad (3)$$

The real (Z_{re}) and imaginary (Z_{im}) components of the impedance were derived as follows:

$$Z_{re} = Z\cos\Phi \quad (4)$$

$$Z_{im} = Z\cos\Phi \quad (5)$$

The corresponding capacitance (C) was calculated using Equation (6):

$$C = (2\pi \mathrm{f} Z_{im})^{-1} \quad (6)$$

where f is the frequency of the AC perturbation. The distribution of relaxation time (DRT) was extracted from the EIS data using the DRT-TOOLS toolbox in MATLAB R2023b, developed by Professor Francesco Ciucci's research group. The toolbox is freely available at: https://github.com/ciuccislab.

Characterizations

Fourier transform infrared (FTIR) spectra were collected using a NICOLET iS50 FT-IR spectrometer. ^{1}H nuclear magnetic resonance (^{1}H NMR) spectra were recorded on a Bruker 600 MHz liquid-state NMR spectrometer. Raman spectra and corresponding mapping images were acquired using a Horiba HR-Evolution Raman microscope with a 532 nm excitation laser. The electrolyte viscosity is measured using the NDJ-5S digital viscometer. The pH values were measured using a Bante210-CN pH meter. Contact angle measurements of various solutions on Zn foil surfaces were performed using a JC2000D5E contact angle goniometer. Transmission electron microscopy (TEM) images were obtained using an FEI Talos F200X G2 microscope operated at 200 kV. X-ray diffraction (XRD) patterns and XRD pole figures were collected using a Rigaku MiniFlex600 and a Rigaku SmartLab diffractometer, respectively, both equipped with Cu Kα radiation sources. X-ray photoelectron spectroscopy (XPS) measurements were conducted on a ThermoFisher ESCALAB 250Xi spectrometer, with all binding energies calibrated to the C 1s peak at 284.8 eV. Scanning electron microscopy (SEM) images were captured using a Nova NanoSEM 450 field-emission SEM. *In situ* optical microscopy (OM) was used to visualize the dynamic nucleation and growth of Zn in different electrolytes. The images were recorded on a Fenye ZLD200-4XC microscope equipped with a digital camera, using a Zn||Cu electrolytic cell operated at a current density of 20 mA cm^{-2}.

Theoretical calculations

Molecular dynamics (MD) simulations: All-atom MD simulations of bulk electrolytes were performed using the GROMACS 2018.3 software.[S3] The electrolyte systems were modeled using the Assisted Model Building and Energy Refinement 3

(AMBER3) force field.[S4] Force field parameters for OTf^- and TM-Urea were generated with AnteChamber Python Parser interfacE (ACPYPE), while parameters for Zn^{2+} were adopted from the built-in GROMACS force field. Water molecules were modeled using the extended simple point charge (SPC/E) model. Electrostatic interactions were treated using the Particle-Mesh Ewald (PME) method, and van der Waals (vdW) interactions were handled using a cutoff scheme with a radius of 10 Å. All simulations were carried out in the NpT ensemble at 298.15 K and 1.01 atm within a cubic box applying periodic boundary conditions in all three Cartesian directions. Each system was initially equilibrated for 10 ns (5,000,000 steps with a 2 fs time step) using a velocity-rescale thermostat and the Berendsen barostat to control temperature and pressure, respectively. Following equilibration, a production run of 10 ns (5,000,000 steps) was performed for data collection. During the production stage, pressure was regulated using the Parrinello-Rahman barostat. Radial distribution functions (RDFs, $g(r)$) were calculated using built-in GROMACS tools, while coordination numbers ($N(r)$) and molecular snapshots were analyzed with the open-source Visual Molecular Dynamics (VMD) software.[S5]

Density functional theory (DFT) calculations: For isolated systems, DFT calculations were conducted using Gaussian 16.[S6] All geometries were optimized using the Becke-3-parameter Lee-Yang-Parr (B3LYP) functional with the 6-31G(d,p) basis set for H, C, N, O, F, and S atoms. The Zn atom was treated using the Stuttgart-Dresden (SDD) pseudopotential. Frequency calculations at the same level were performed to confirm that each optimized structure corresponds to a true minimum (*i.e.*, no imaginary frequencies). For periodic systems, DFT calculations were carried out using the Vienna Ab initio Simulation Package (VASP).[S7] Core electrons were described with projector augmented wave (PAW) pseudopotentials,[S8] and the exchange-correlation functional was treated using the Perdew-Burke-Ernzerhof (PBE) generalized-gradient approximation (GGA).[S9] A plane-wave energy cutoff of 450 eV was applied. Brillouin zone sampling was performed using a Γ-centered Monkhorst-Pack k-point mesh of 2 × 2 × 2. The convergence criteria were set to 10^{-5} eV for electronic energy and 0.02 eV·$Å^{-1}$ for forces during geometry optimization.

Supplementary Figures and Tables

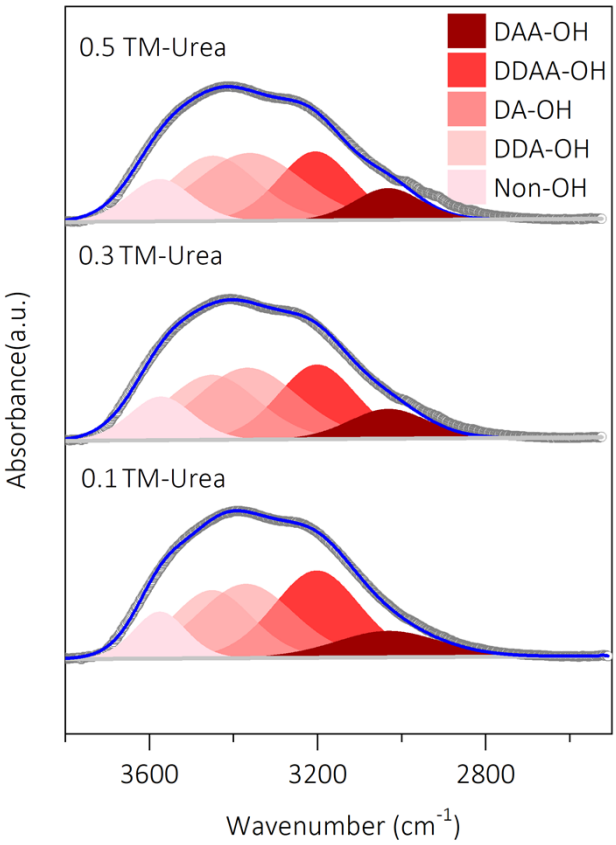

Fig. S1 Deconvoluted FTIR spectra of O–H stretching vibrations in 0.1-0.5 TM-Urea electrolytes, representing water molecules engaged in different HB environments: DAA-OH, DDAA-OH, DA-OH, DDA-OH, and Non-OH.

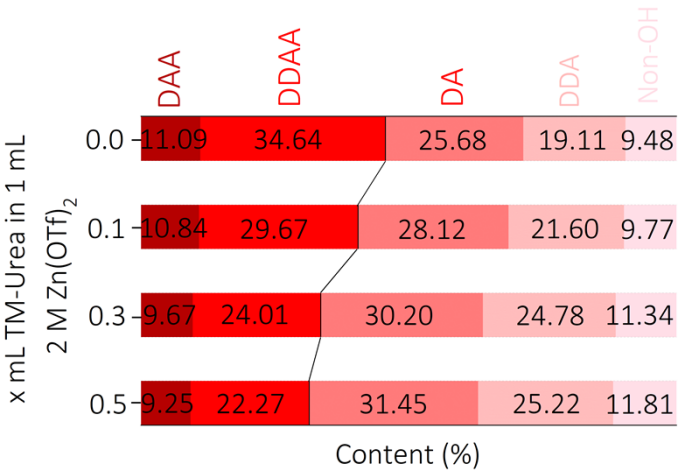

Fig. S2 Relative proportions of DAA, DDAA, DA, DDA, and Non-OH species in 2 M $Zn(OTf)_2$ and 0.1–0.5 TM-Urea electrolytes.

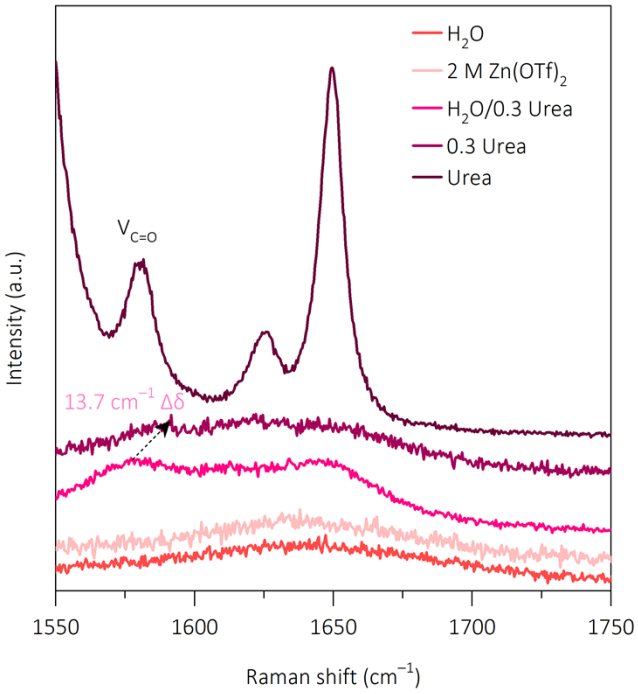

Fig. S3 Raman spectra of the C=O stretching region for Urea in different solutions.

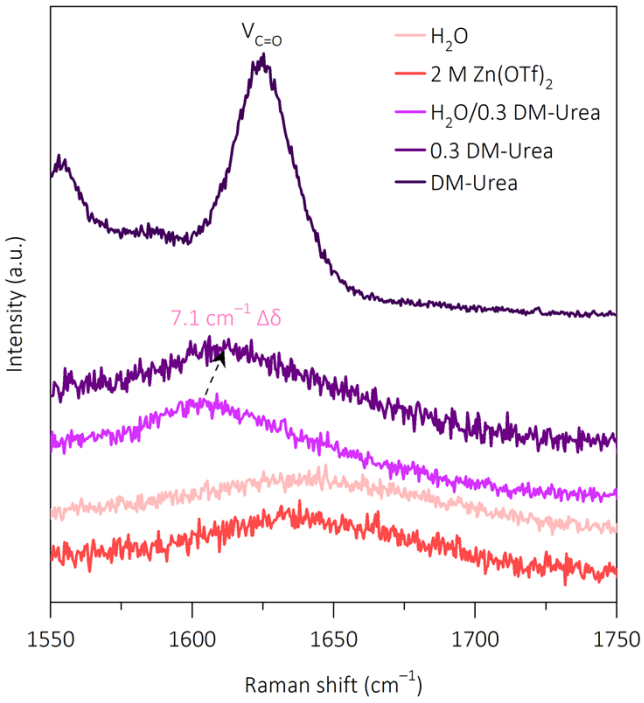

Fig. S4 Raman spectra of the C=O stretching region for DM-Urea in various solutions.

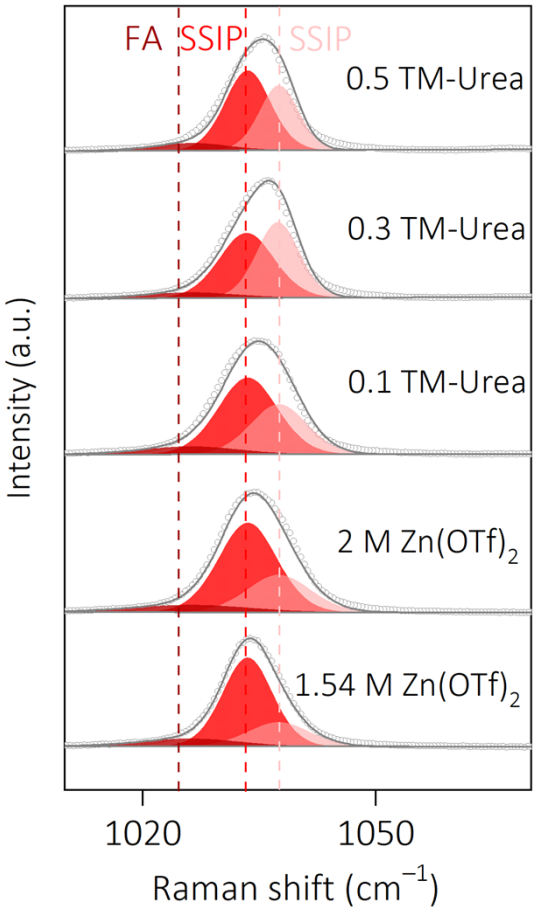

Fig. S5 Peak-fitted Raman spectra of various electrolytes at 1020–1050 cm^{-1}.

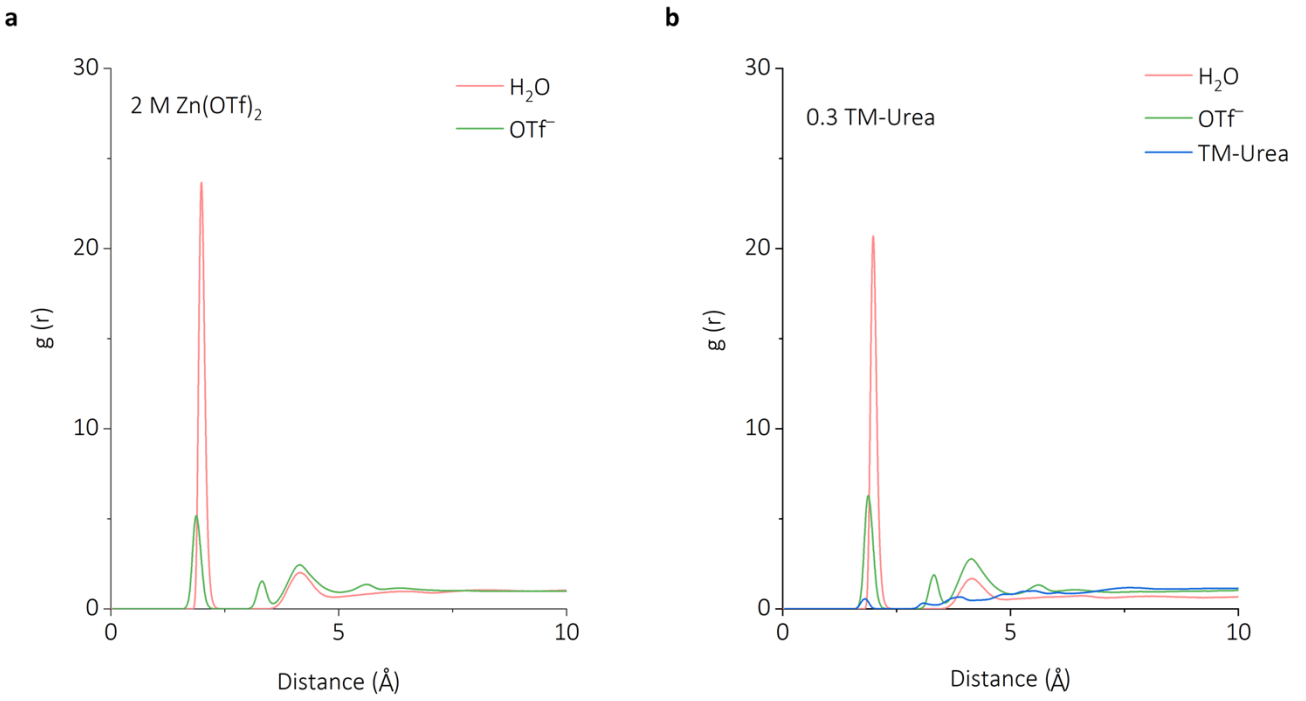

Fig. S6 The $g(r)$ of Zn^{2+} with other species in electrolytes.

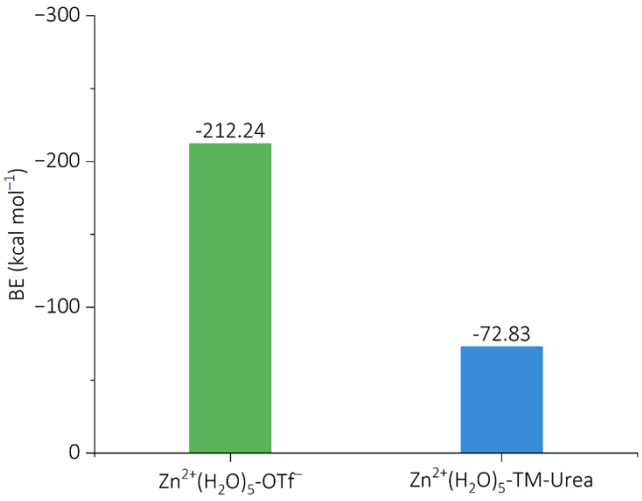

Fig. S7 BE of $Zn^{2+}(H_2O)_5$ with OTf^- and TM-Urea.

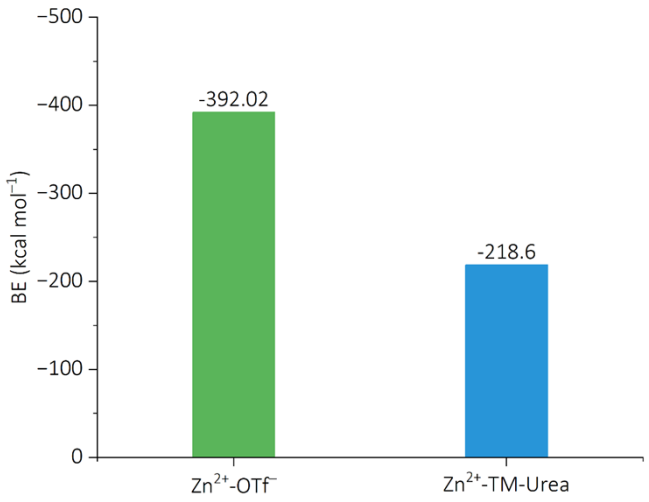

Fig. S8 BE of Zn^{2+} with OTf^{-} and TM-Urea.

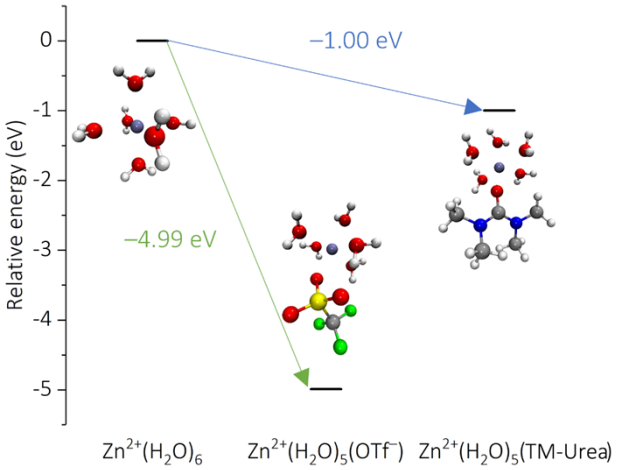

Fig. S9 Substitution energy for replacing one H_2O in $Zn^{2+}(H_2O)_6$ with either OTf^- or TM-Urea.

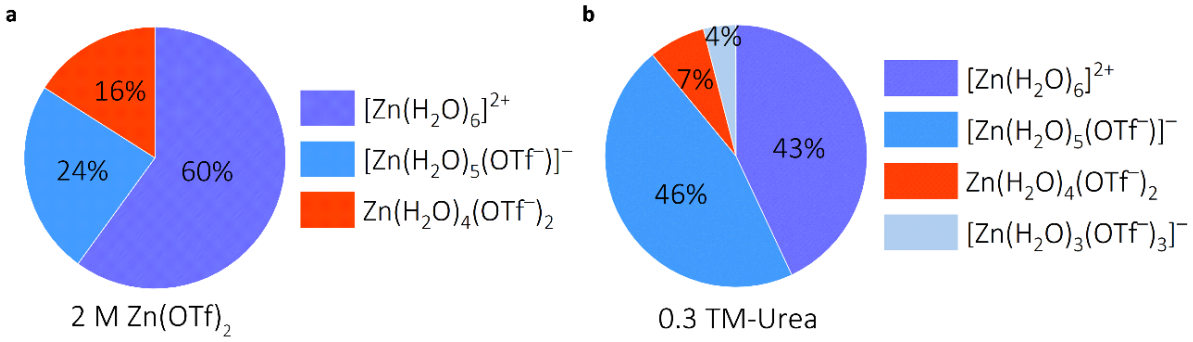

Fig. S10 Distributions of possible Zn^{2+}-solvation compositions of (a) 2 M $Zn(OTf)_2$ and (b) 0.3 TM-Urea from MD simulations.

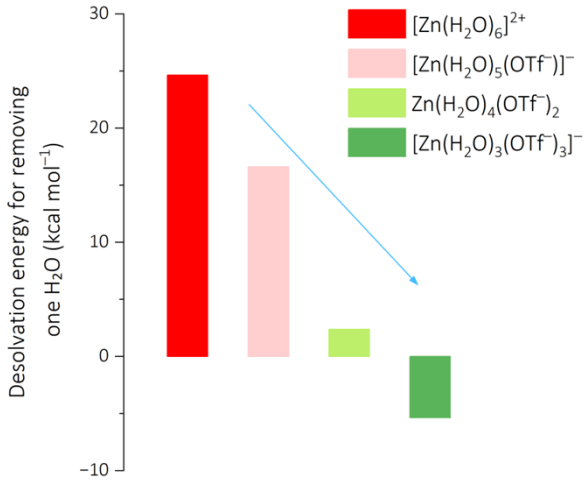

Fig. S11 Desolvation energies for removal of one H_2O molecule from Zn^{2+}-solvation structures.

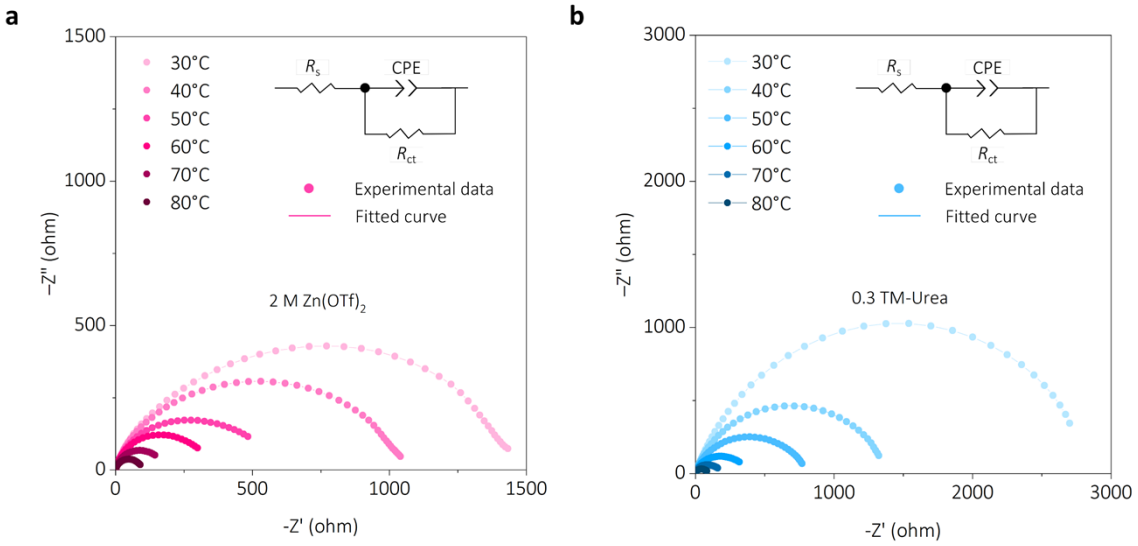

Fig. S12 EIS curves of Zn||Zn symmetrical cells in (a) 2 M $Zn(OTf)_2$ and (b) 0.3 TM-Urea electrolytes over the frequency range of 0.1 Hz to 100 kHz at temperature intervals of 10 °C between 30 and 80 °C. EIS tests were performed without applying any voltage or current. Insets are the corresponding equivalent circuits, where R_s represents the internal resistance arising from the electrolyte, separator, and electrical contacts; R_{ct} denotes the Faradaic charge-transfer resistance at the interfaces; and CPE is the double layer capacitance.

The E_a of Zn electrodes in different electrolytes is determined from Nyquist plots of Zn||Zn cells by analyzing the temperature-dependent R_{ct}.[S10] E_a is calculated from the slope of the linear fit of $\ln(1/R_{ct})$ *vs*. 1000/T.

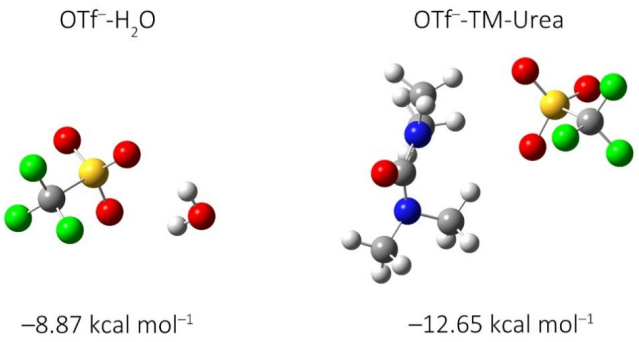

Fig. S13 BE of OTf^- with H_2O and TM-Urea.

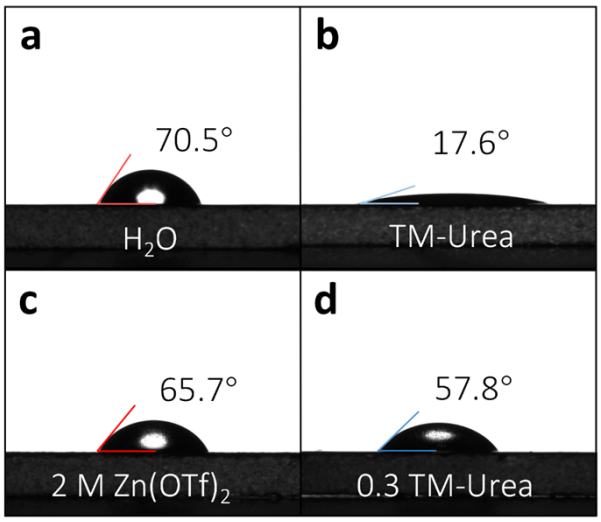

Fig. S14 Contact angle measurements of (a) pure H_2O, (b) TM-Urea as well as (c) 2 M $Zn(OTf)_2$ and (d) 0.3 TM-Urea electrolytes droplets on the bare Zn.

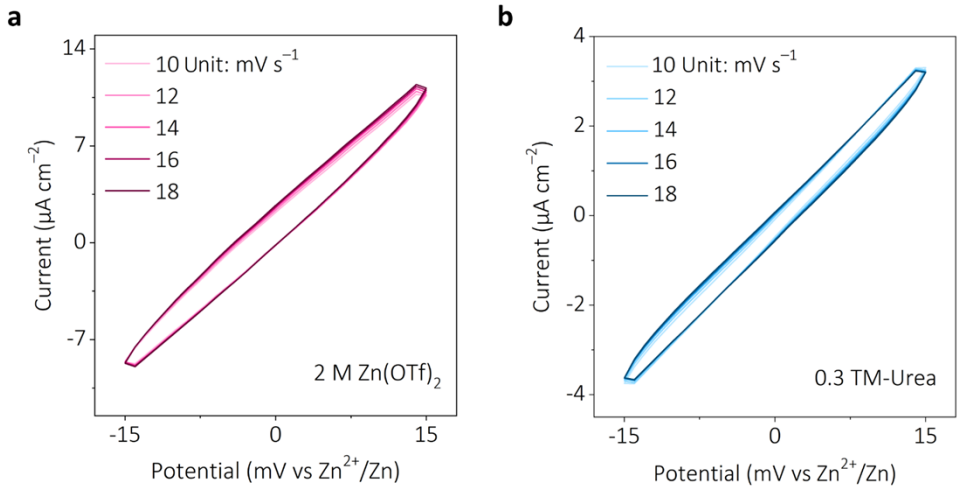

Fig. S15 CV curves for Zn||Zn symmetric cells using (a) 2 M $Zn(OTf)_2$ and (b) 0.3 TM-Urea electrolytes in a voltage range of −15 mV to 15 mV (non-Faradaic region) under various scanning rates.

The EDL capacitance is calculated using the equation of $C=i/v$, where C is the capacitance, i is the current, and v is the scan rate. i is defined as half the difference between the anodic and cathodic currents at each scan rate.[S11]

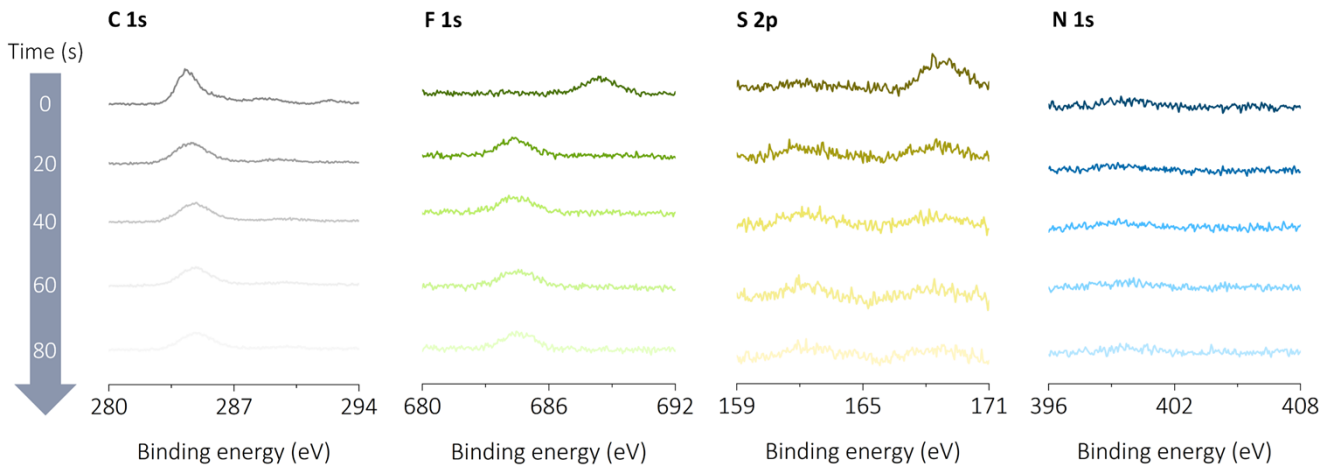

Fig. S16 XPS depth profiles of the Zn anode cycled in the 2 M $Zn(OTf)_2$ electrolyte (10 cycles at 5 mA cm^{-2}, 5 mAh cm^{-2}), showing the evolution of C 1s, F 1s, S 2p, and N 1s signals with Ar^+ sputtering time (0–80 s).

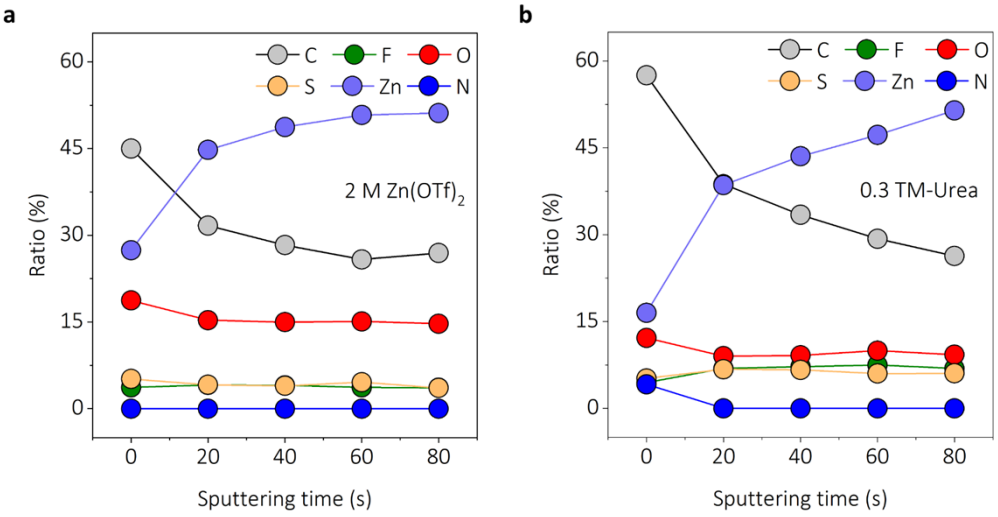

Fig. S17 Atomic composition ratios of the SEI on cycled Zn electrodes in (a) 2 M $Zn(OTf)_2$ and (b) 0.3 TM-Urea electrolytes at various Ar^+ sputtering times.

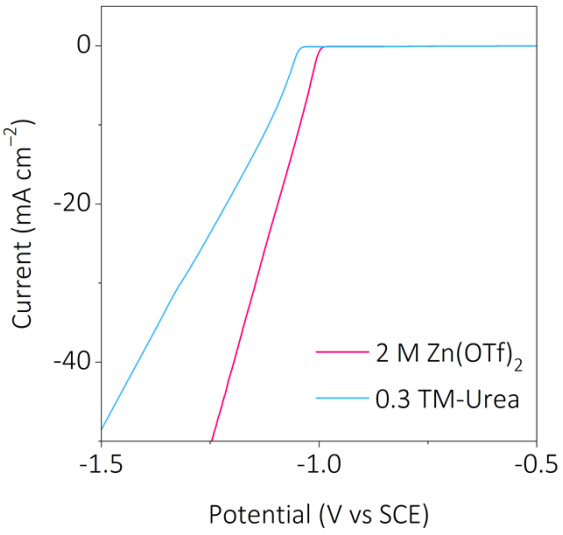

Fig. S18 LSV curves of 2 M $Zn(OTf)_2$ and 0.3 TM-Urea electrolytes at 1 mV s^{-1}.

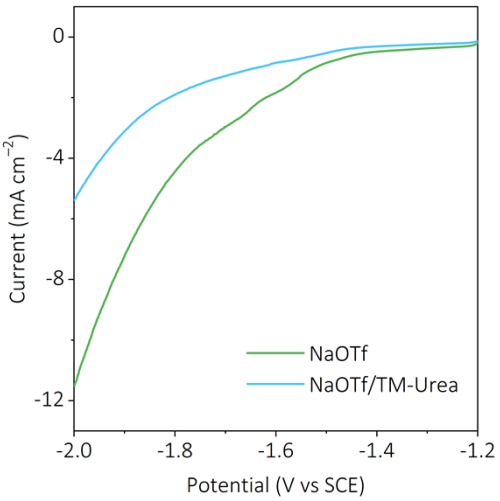

Fig. S19 LSV curves of NaOTf and NaOTf/TM-Urea electrolytes measured at 1 mV s^{-1}, using Zn foil as the working electrode, Ti foil as the counter electrode, and a SCE as the reference electrode.

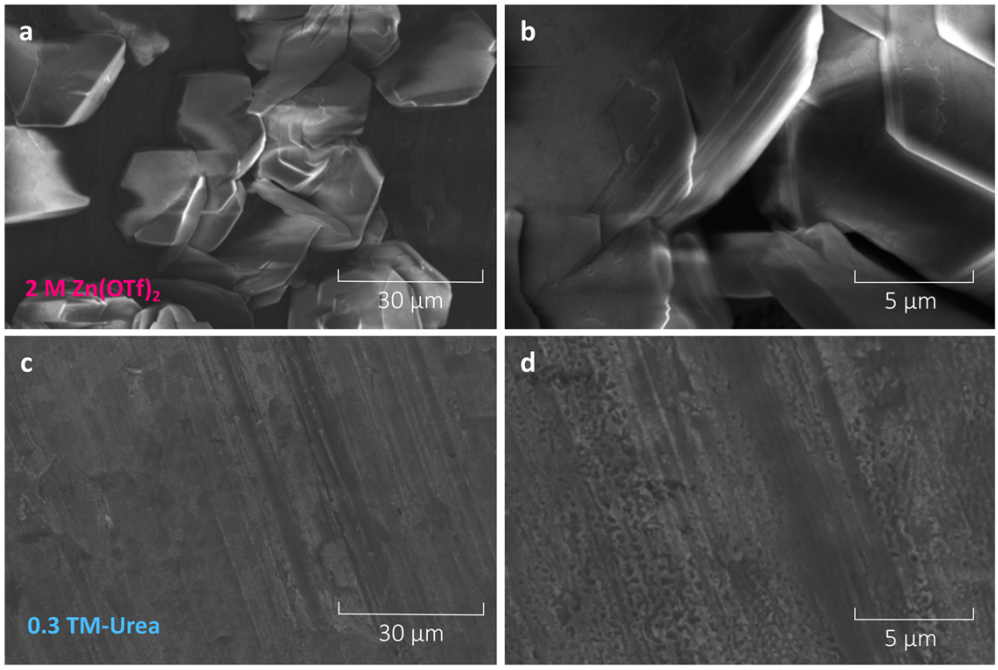

Fig. S20 SEM images of Zn electrodes after 3 days of soaking in (a,b) 2 M $Zn(OTf)_2$ and (c,d) 0.3 TM-Urea electrolytes. Scale bars: 30 µm in (a,c) and 5 µm in (b,d) (magnified view).

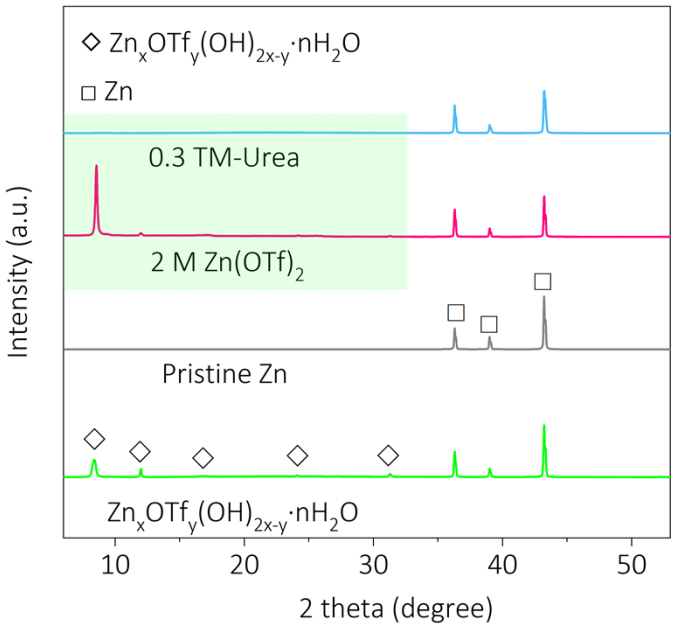

Fig. S21 XRD patterns of Zn foils after soaking in various electrolytes for 3 days.

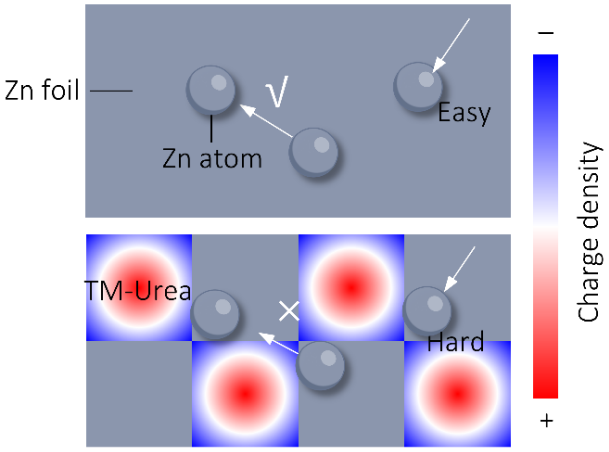

Fig. S22 TM-Urea adsorbed on the Zn anode surface regulates Zn^{2+} diffusion from 2D to 3D.

As illustrated, we provide a schematic showing the deposition mode of Zn with and without TM-Urea adsorption on the Zn surface. Once TM-Urea adsorbs on the Zn surface, it forms a mesh-like structure that inhibits 2D diffusion of Zn^{2+}, thereby suppressing dendrite formation.

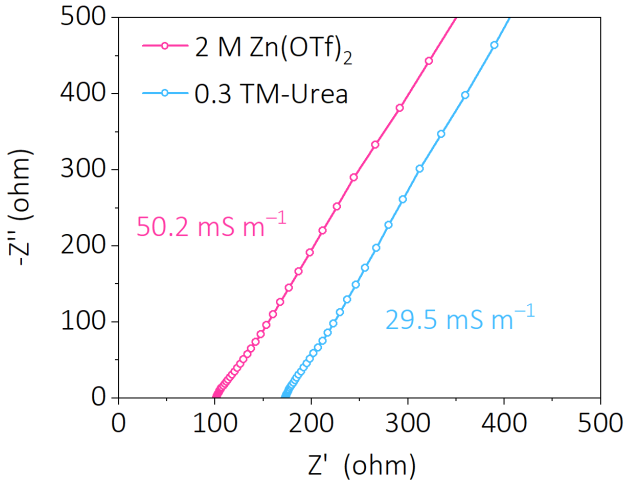

Fig. S23 Nyquist plots of the 2 M $Zn(OTf)_2$ and 0.3 TM-Urea electrolytes measured over the frequency range of 100 kHz to 0.1 Hz for calculating the ionic conductivity.

The ionic conductivity (σ) was calculated using:

$$\sigma = \frac{L}{R_b S}$$

where R_b is the bulk resistance obtained from EIS fitting, L is the thickness of the electrode–electrode (1 cm), and S is the electrode–electrolyte contact area (0.196 cm^2).

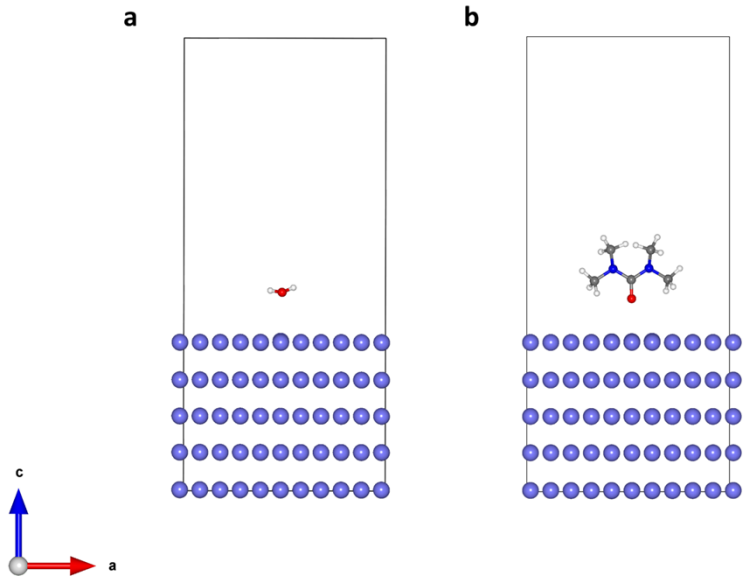

Fig. S24 Models of the Zn(002) surface with (a) H_2O or (b) TM-Urea adsorption.

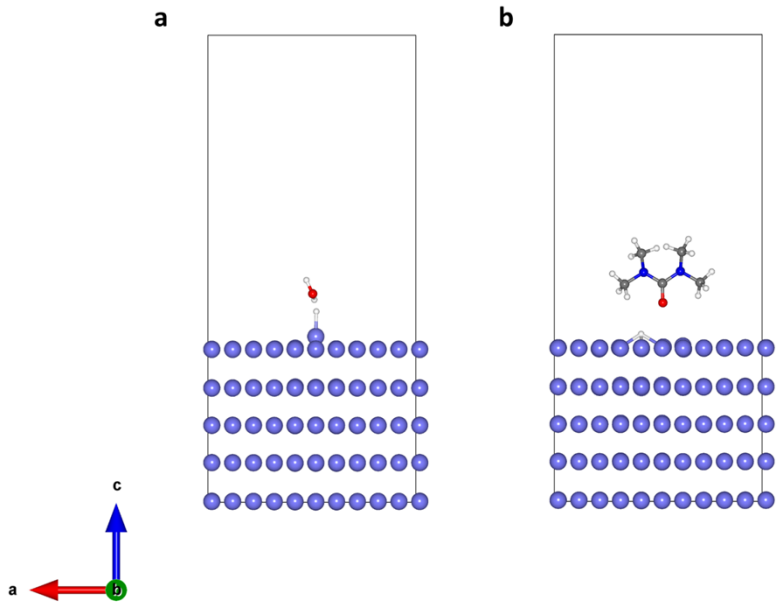

Fig. S25 Adsorption models of a single H atom on the Zn(002) surface with (a) H_2O and (b) TM-Urea.

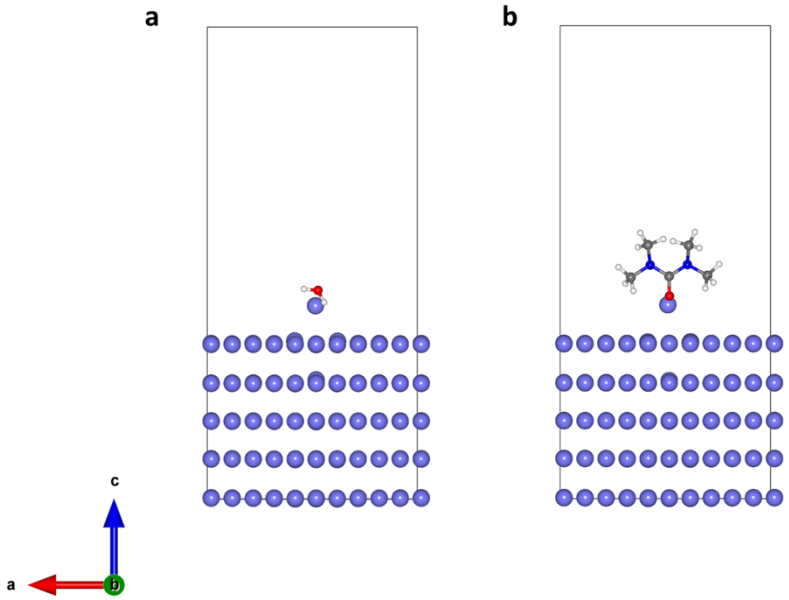

Fig. S26 Adsorption models of a single Zn atom on the Zn(002) surface with (a) H_2O and (b) TM-Urea.

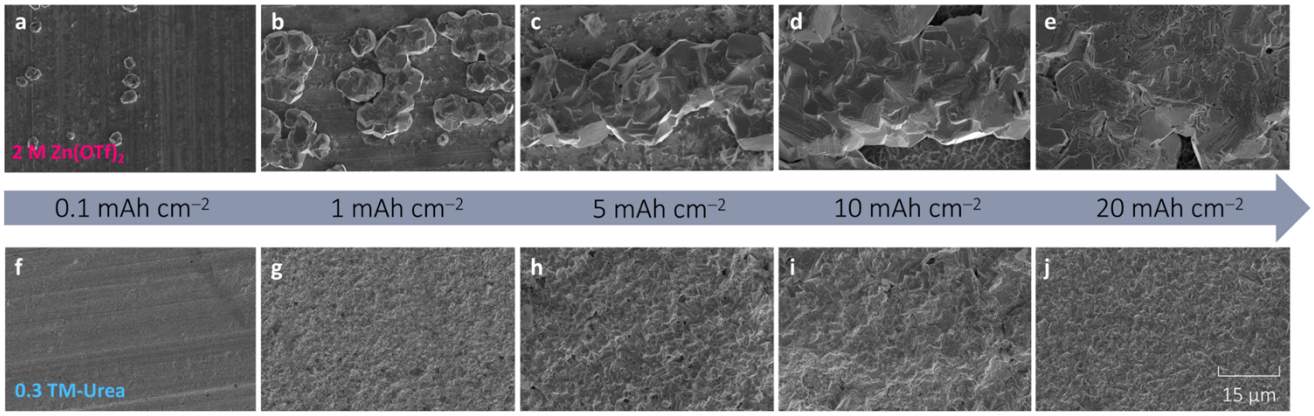

Fig. S27 SEM images of electrodeposited Zn in (a-d) 2 M $Zn(OTf)_2$ and (e-h) 0.3 TM-Urea electrolytes at different plating capacities under 20 mA cm^{-2}. Scale bar: 15 µm in (a-h).

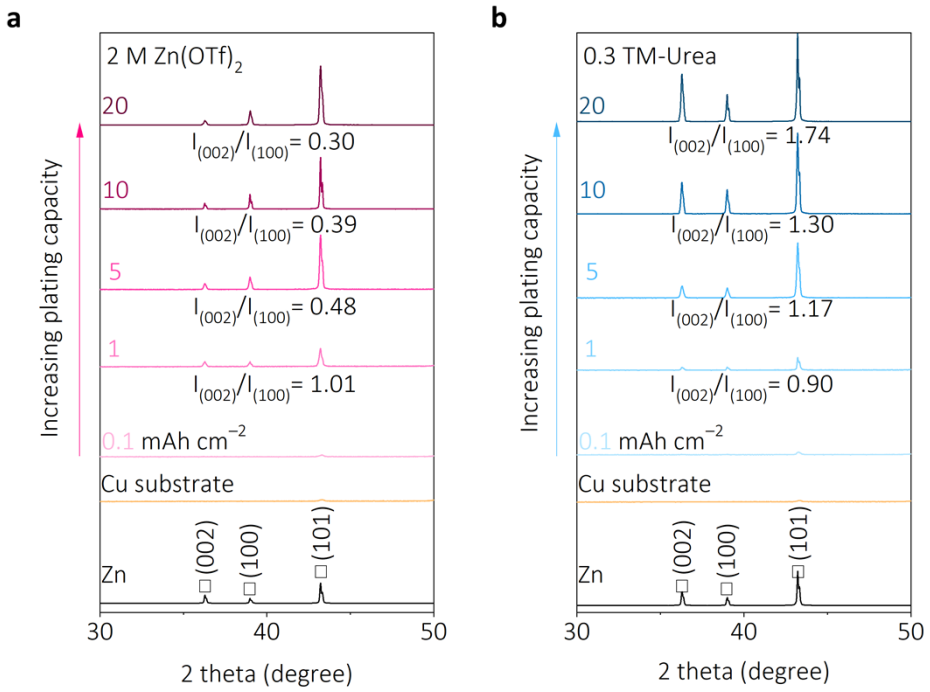

Fig. S28 XRD patterns of Zn electrodeposits in (a) 2 M $Zn(OTf)_2$ and (b) 0.3 TM-Urea electrolytes at varying plating capacity at 20 mA cm^{-2}.

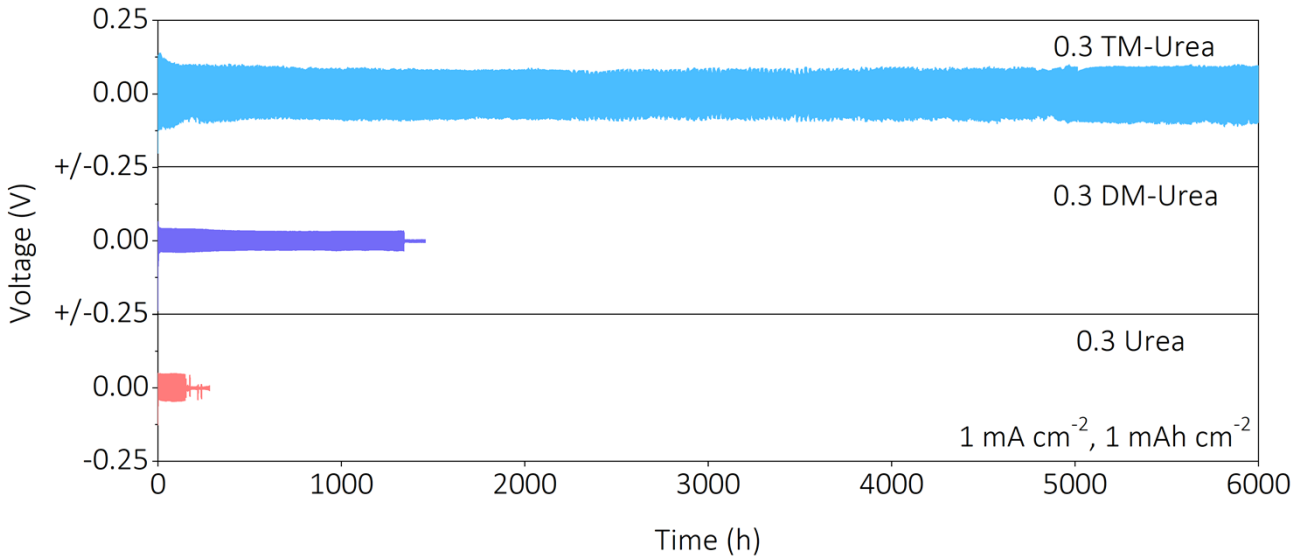

Fig. S29 Cycling performance of Zn||Zn symmetric cells with 0.3 urea-based electrolytes at 1 mA cm^{-2}, 1 mAh cm^{-2}.

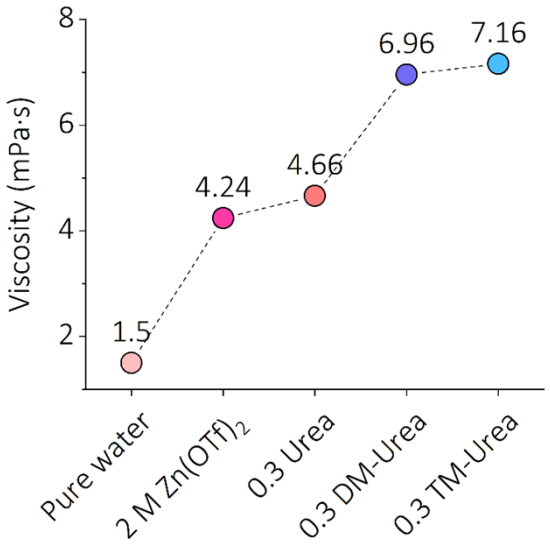

Fig. S30 Viscosities of pure water as well as 2 M $Zn(OTf)_2$ and 0.3 Urea (DM-Urea or TM-Urea) electrolytes.

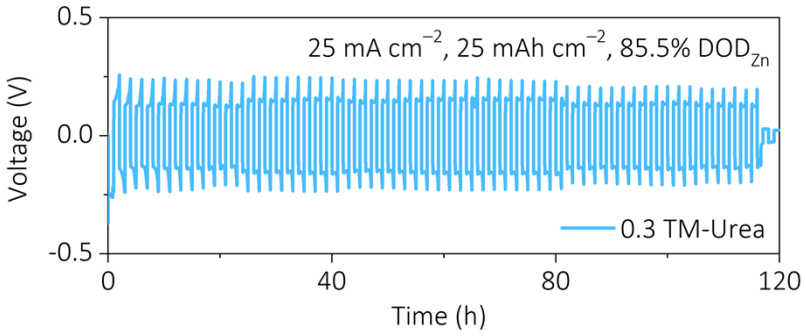

Fig. S31 Cycling performance of Zn||Zn symmetric cells with the 0.3 TM-Urea electrolyte at 25 mA cm^{-2}, 25 mAh cm^{-2}.

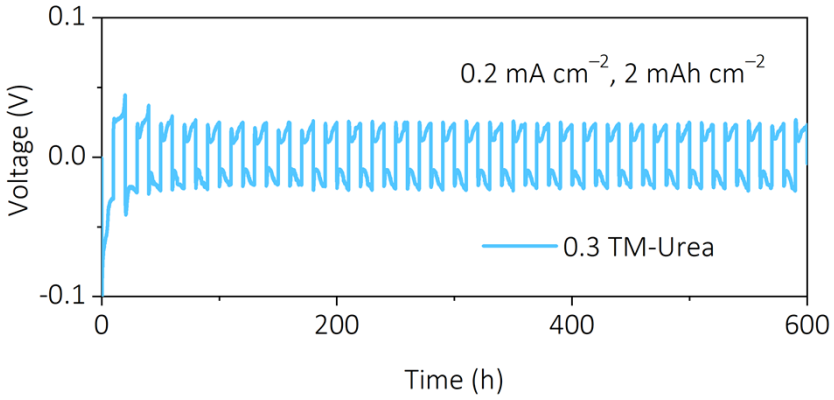

Fig. S32 Cycling performance of Zn||Zn symmetric cells with the 0.3 TM-Urea electrolyte at 0.2 mA cm^{-2}, 2 mAh cm^{-2}.

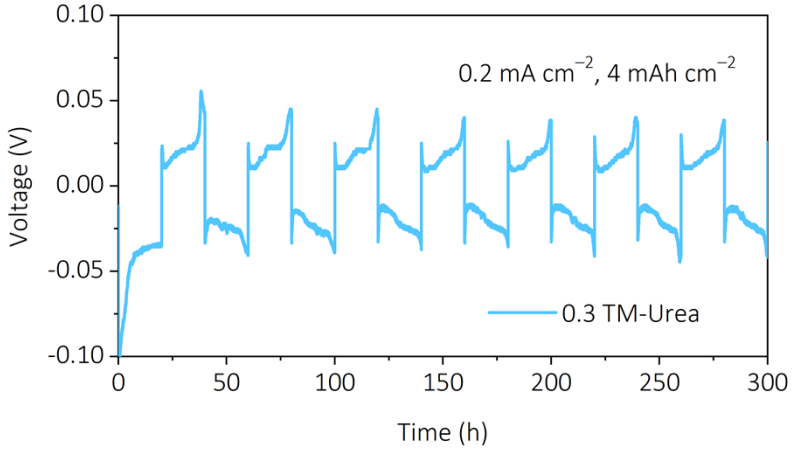

Fig. S33 Cycling performance of Zn||Zn symmetric cells with the 0.3 TM-Urea electrolyte at 0.2 mA cm^{-2}, 4 mAh cm^{-2}.

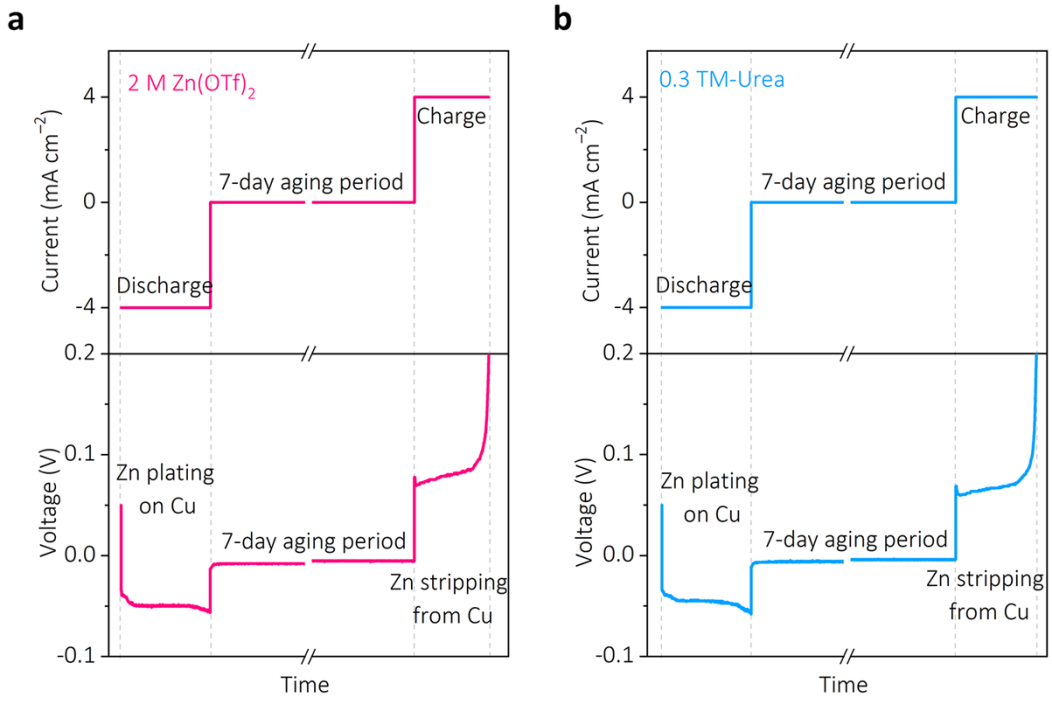

Fig. S34 Electrochemical test procedure for quantifying aging-induced capacity loss for Zn||Cu cells using 2 M $Zn(OTf)_2$ and 0.3 TM-Urea electrolytes.

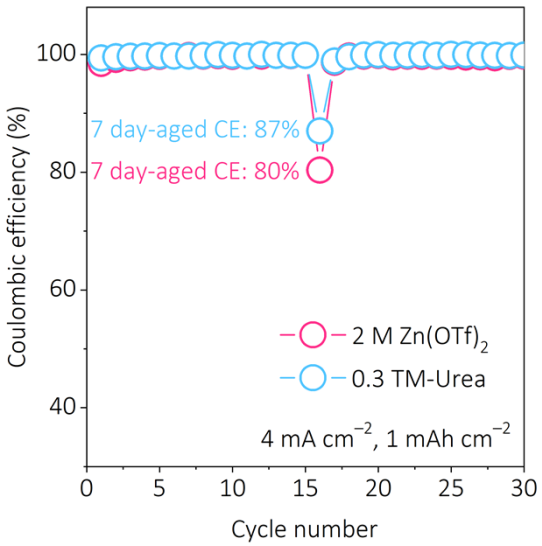

Fig. S35 CE of Zn||Cu cells using electrolytes with/without TM-Urea including the 7-day aging procedure.

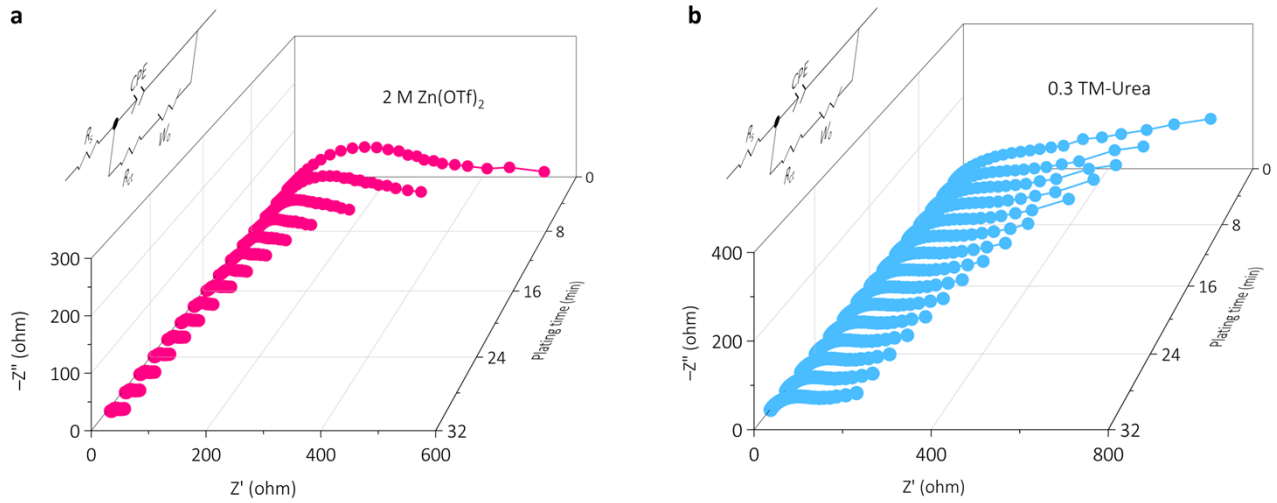

Fig. S36 Nyquist plots of the Zn||Zn symmetrical cells during the plating process using (a) 2 M $Zn(OTf)_2$ and (b) 0.3 TM-Urea electrolytes at 5 mA cm^{-2}, measured over time. The corresponding equivalent circuits are shown, where R_s represents the internal resistance arising from the electrolyte, separator, and electrical contacts; R_{ct} denotes the Faradaic charge-transfer resistance at the interfaces; CPE is the double layer capacitance; and W_o corresponds to the Warburg impedance associated with ion diffusion into the electrodes. For the EIS measurements, Zn||Zn cells undergo a 2-min discharge at 5 mA cm^{-2} followed by a 2-min rest, and this process is repeated 15 times.

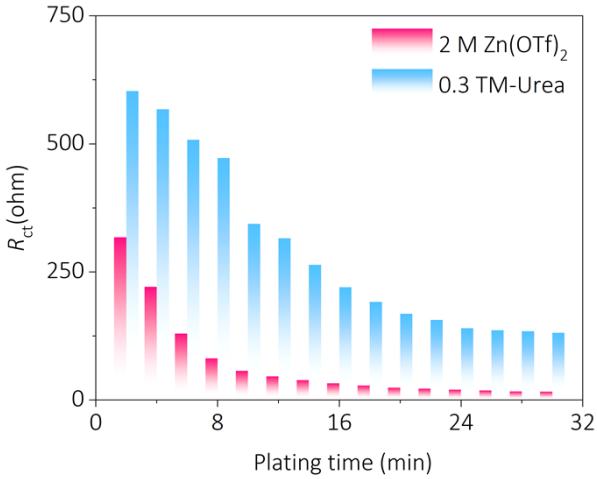

Fig. S37 The R_{ct} values obtained by fitting the Nyquist plots using the equivalent circuits.

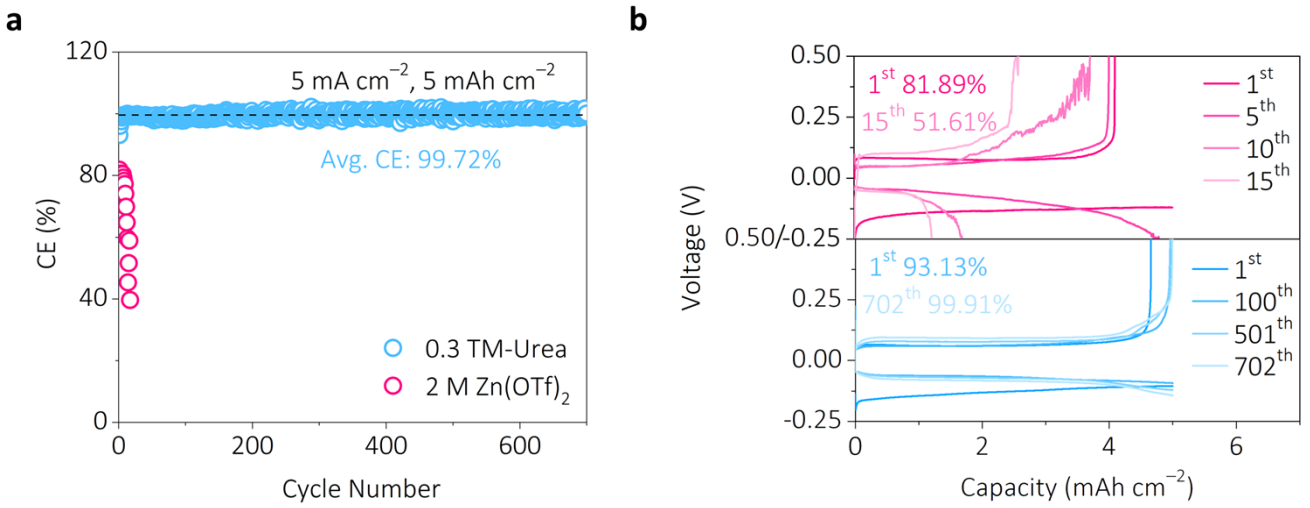

Fig. S38 (a) CE measurements of Zn||Cu cells using different electrolytes, and (b) the corresponding voltage profiles at different cycles.

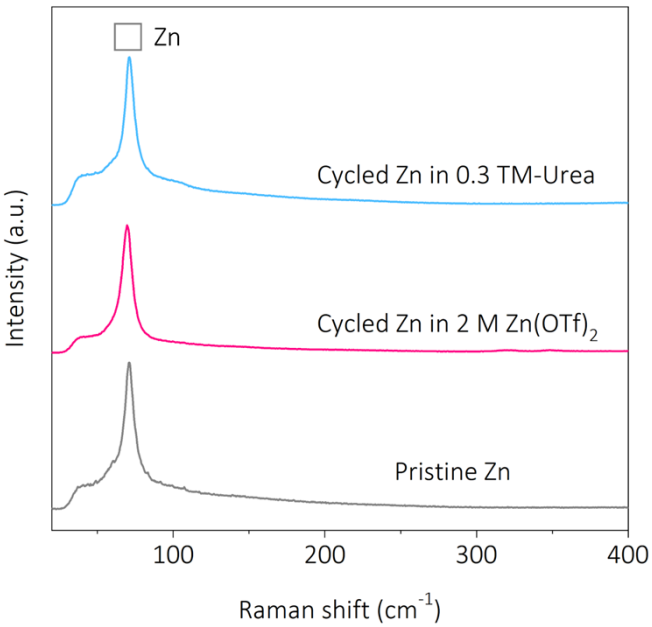

Fig. S39 Raman spectra of pristine Zn and cycled Zn in different electrolytes. The Raman peak observed at 71 cm^{-1} is attributed to the E_{2g} mode of Zn metal.

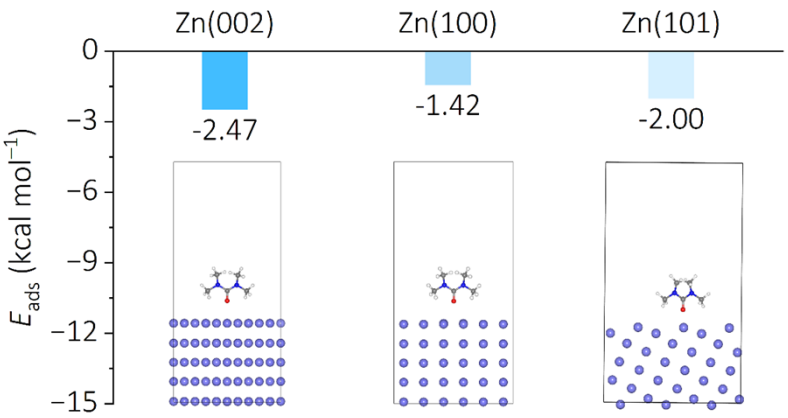

Fig. S40 Adsorption models of a TM-Urea molecule on Zn-(002, 100, 101) facets and the corresponding E_{ads}.

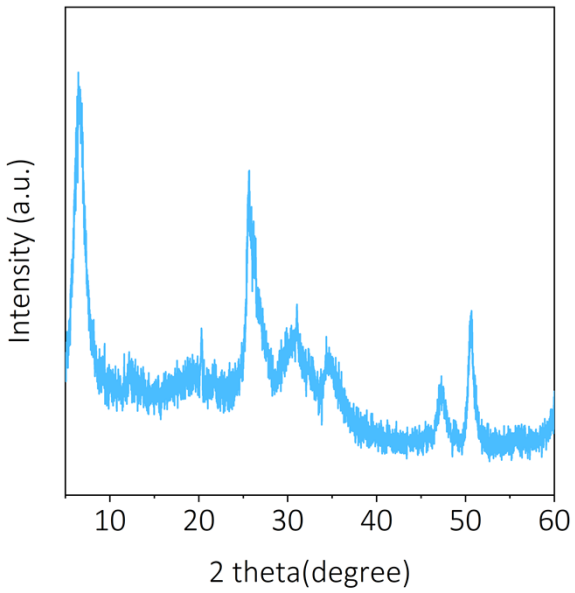

Fig. S41 XRD pattern of the as-prepared VOH material.

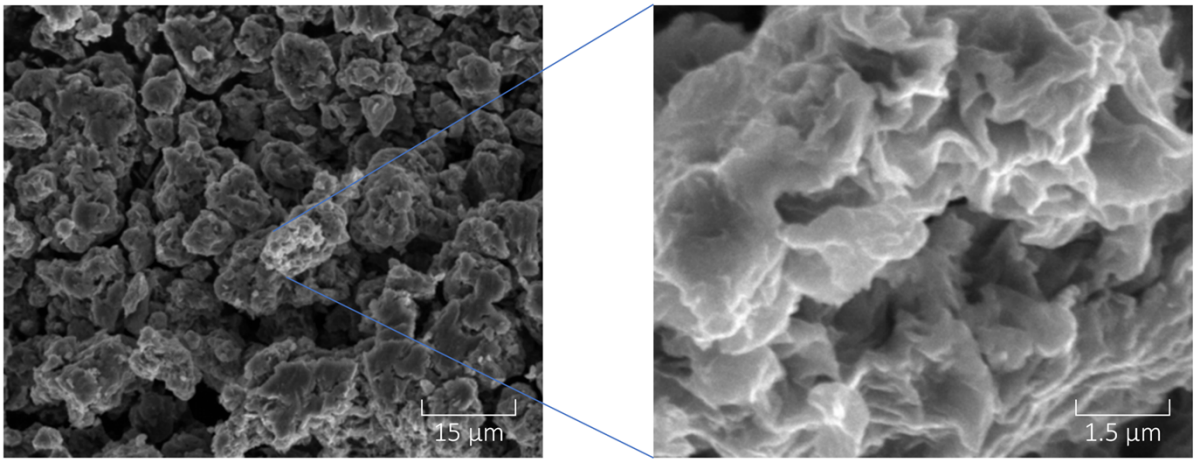

Fig. S42 SEM images of the as-prepared VOH material.

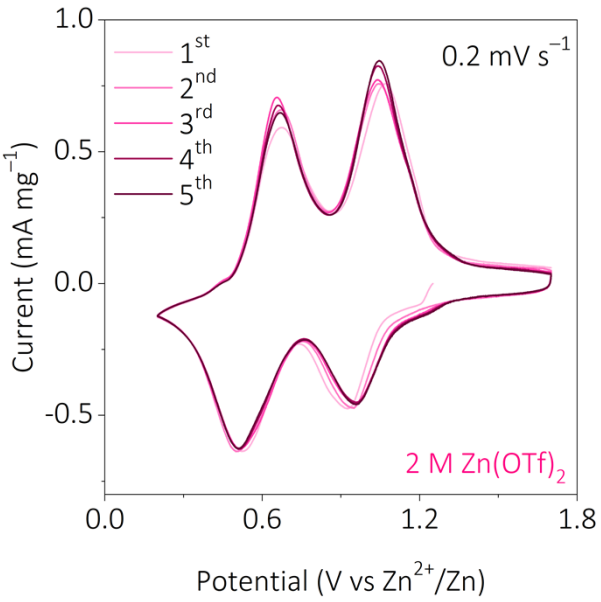

Fig. S43 CV curves of full cells in the 2 M $Zn(OTf)_2$ electrolyte at a scan rate of 0.2 mV s^{-1}.

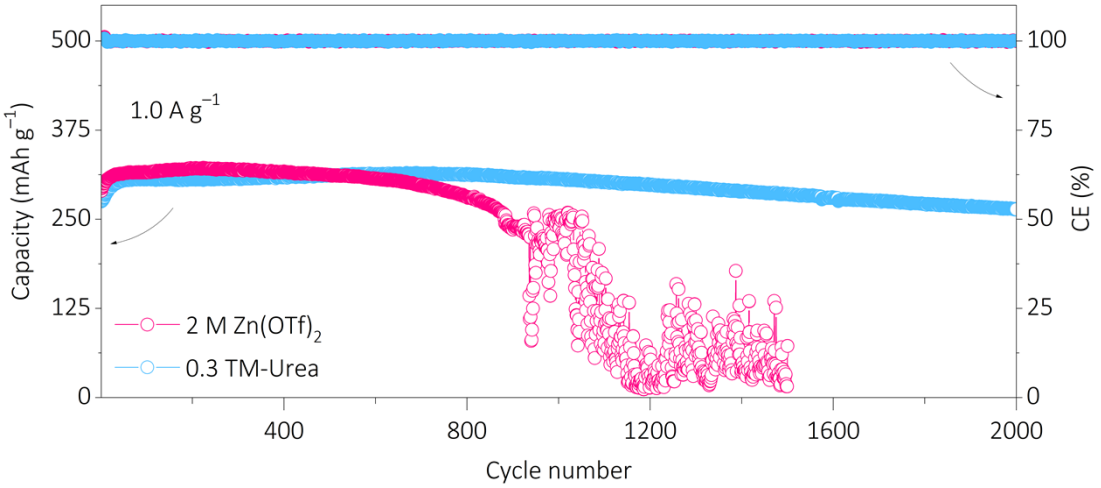

Fig. S44 Long-term cycling stability of full cells in different electrolytes at 1.0 A g^{-1}.

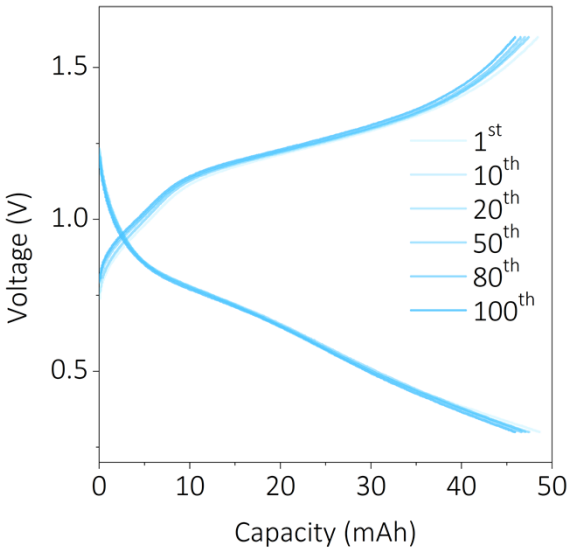

Fig. S45 Typical charge/discharge curves of the pouch-type full cell in the 0.3 TM-Urea electrolyte at a testing current of 96 mA.

Tab. S1 Electrolyte formulations and their abbreviations used in this work.

Electrolytes	Preparation details	Molarity ($Zn(OTf)_2$ + ureas)
2 M $Zn(OTf)_2$	Adding 1.0397g of $Zn(OTf)_2$ into 1 mL of deionized water	2 M + 0 M
0.1 TM-Urea	Adding 0.1 mL of TM-Urea solvent (0.83 mmol) into 1 mL of the 2 M $Zn(OTf)_2$	1.82 M + 0.76 M
0.3 TM-Urea	Adding 0.3 mL of TM-Urea solvent (2.50 mmol) into 1 mL of the 2 M $Zn(OTf)_2$	1.54 M + 1.92 M
0.5 TM-Urea	Adding 0.5 mL of TM-Urea solvent (4.17 mmol) into 1 mL of the 2 M $Zn(OTf)_2$	1.33 M + 2.78 M
0.3 Urea	Adding 2.50 mmol Urea powder into 1 mL of the 2 M $Zn(OTf)_2$	1.79 M + 2.23 M
0.3 DM-Urea	Adding 2.50 mmol DM-Urea powder into 1 mL of the 2 M $Zn(OTf)_2$	1.67 M + 2.08 M

Tab. S2 pH values of 2 M $Zn(OTf)_2$ and 0.1–0.5 TM-Urea electrolytes at 25 °C.

Electrolytes	pH-1	pH-2	pH-3	Avg. pH
2 M $Zn(OTf)_2$	3.50	3.51	3.52	3.51
0.1 TM-Urea	3.91	3.92	3.93	3.92
0.3 TM-Urea	4.10	4.14	4.16	4.13
0.5 TM-Urea	4.52	4.54	4.54	4.53

Tab.S3 Cycling stability comparison of Zn||Zn symmetric cells between this work and the reported literature.

Additives	Thickness and theoretical capacity	Electrolyte	Cumulative capacity/ Current density (Ah cm^{-2}/mA cm^{-2})	DOD (%)	Ref.
TM-Urea	**50 µm ~29.25 mAh**	**0.3 TM-Urea**	**21.75/5** **35/10** **8/20** **2.5/25**	**17.09** **34.19** **68.38** **85.47**	**This work**
PMS	100 µm ~58.5 mAh	2 M $ZnSO_4$ + 20 mM $HSC_3H_6SO_3Na$	7/10	17.09	S12
FF	25 µm ~14.625 mAh	1 m $Zn(TFSI)_2$ + 0.5 m trifluoroethyl formate/DMSO-H_2O (mass ratio: DMSO: H_2O = 4: 1)	3.8/2	13.68	S13
EC	10 µm ~5.85 mAh	2 M $Zn(OTf)_2$ / EC-H_2O (volume ratio: EC: H_2O = 5: 5)	2/1	17.09	S14
BHED	100 µm ~58.5 mAh	2 M $ZnSO_4$ + 4 mM bis(2-hydroxyethyl) disulfide	3/10	25.5	S15
MA	60 µm ~35.1 mAh	2 M $ZnSO_4$ + 5 wt.% maleic anhydride	2.7/10	28.49	S16
NADS	250 µm ~146.25 mAh	2 M $ZnSO_4$-1.5 mM 26 naphthalenedisulfonic acid disodium salt	15/30	3.42	S17
TEGDME	~30 µm ~17.55 mAh	1 m $Zn(BF_4)_2$ + 0.2 m $Zn(CH_3COO)_2$ / TEGDME-H_2O (molar ratio: TEGDME: H_2O=40:1)	1.878/6.26	20	S18
BHEG	100 µm ~58.5 mAh	2 M $ZnSO_4$ + 0.5 M N,N-bis(2-hydroxyethyl)glycine	3/5	8.5	S19

ZSO-SAA	80 µm ~46.8 mAh	2 M $ZnSO_4$ + 0.01 wt.% saponin+ 0.03 wt.% anisaldehyde	17/10	10.68	S20
PNO	100 µm ~58.5 mAh	2 M $ZnSO_4$ + 0.03 M pyridine nitrogen oxides	5/5	8.55	S21
DMSO	20 µm ~11.7 mAh	0.5 M $Zn(BF_4)_2.xH_2O$-DMSO	0.6/1	60	S22
SL	50 µm ~29.25 mAh	1 m $Zn(ClO_4)_2$/SL-H_2O (mass ratio: SL: H_2O = 1: 4)	1.3/1	3.42	S23
N-ac	100 µm ~58.5 mAh	2 M $ZnSO_4$ + 0.1 M N-Acetyl-ε-caprolactam	12/10	17.09	S24
CNF	100 µm ~58.5 mAh	3 M $ZnSO_4$/trifluoroacetamide (CNF) (volume ratio: CNF: $ZnSO_4$ = 3: 7)	25/20	3.42	S25
q-GPA	~35 µm ~20.475 mAh	1 M $Zn(OTf)_2$ + 8 mg/mL quaternized galactomannan polysaccharide	18.6/20	48.7	S26

Supplementary References

[S1] H. Wang, X. Bi, Y. Bai, C. Wu, S. Gu, S. Chen, F. Wu, K. Amine and J. Lu, *Adv. Energy Mater.*, 2017, **7**, 1602720.

[S2] A. Moretti, F. Maroni, I. Osada, F. Nobili and S. Passerini, *ChemElectroChem*, 2015, **2**, 529-537.

[S3] H. J. Berendsen, D. van der Spoel and R. van Drunen, *Comp. Phys. Comm.*, 1995, **91**, 43-56.

[S4] Y. Duan, C. Wu, S. Chowdhury, M. C. Lee, G. Xiong, W. Zhang, R. Yang, P. Cieplak, R. Luo and T. Lee, *J. Comput. Chem.*, 2003, **24**, 1999-2012.

[S5] W. Humphrey, A. Dalke and K. Schulten, *J. Mol. Graph.*, 1996, **14**, 33-38.

[S6] M. J. Frisch, G. W. Trucks, H. B. Schlegel, G. E. Scuseria, M. A. Robb, J. R. Cheeseman, G. Scalmani, V. Barone, G. A. Petersson, H. Nakatsuji, X. Li, M. Caricato, A. V. Marenich, J. Bloino, B. G. Janesko, R. Gomperts, B. Mennucci, H. P. Hratchian, J. V. Ortiz, A. F. Izmaylov, J. L. Sonnenberg, D. Williams-Young, F. Ding, F. Lipparini, F. Egidi, J. Goings, B. Peng, A. Petrone, T. Henderson, D. Ranasinghe, V. G. Zakrzewski, J. Gao, N. Rega, G. Zheng, W. Liang, M. Hada, M. Ehara, K. Toyota, R. Fukuda, J. Hasegawa, M. Ishida, T. Nakajima, Y. Honda, O. Kitao, H. Nakai, T. Vreven, K. Throssell, J. A. Montgomery, Jr., J. E. Peralta, F. Ogliaro, M. J. Bearpark, J. J. Heyd, E. N. Brothers, K. N. Kudin, V. N. Staroverov, T. A. Keith, R. Kobayashi, J. Normand, K. Raghavachari, A. P. Rendell, J. C. Burant, S. S. Iyengar, J. Tomasi, M. Cossi, J. M. Millam, M. Klene, C. Adamo, R. Cammi, J. W. Ochterski, R. L. Martin, K. Morokuma, O. Farkas, J. B. Foresman and D. J. Fox, *Gaussian 16, Revision B.01*, Gaussian, Inc., Wallingford, CT, 2019.

[S7] G. Kresse and J. Furthmüller, *Phys. Rev. B*, 1996, **54**, 11169.

[S8] G. Kresse and D. Joubert, *Phys. Rev. B*, 1999, **59**, 1758.

[S9] J. P. Perdew, K. Burke and M. Ernzerhof, *Phys. Rev. Lett*., 1996, **77**, 3865.

[S10] K. Qiu, G. Ma, Y. Wang, M. Liu, M. Zhang, X. Li, X. Qu, W. Yuan, X. Nie and N. Zhang, *Adv. Funct. Mater.*, 2024, **34**, 2313358.

[S11] G. Ma, W. Yuan, X. Li, T. Bi, L. Niu, Y. Wang, M. Liu, Y. Wang, Z. Shen and N. Zhang, *Adv. Mater.*, 2024, **36**, 2408287.

[S12] Y. Song, M. Chen, Z. Zhong, Z. Liu, S. Liang and G. Fang, *Nat. Commun.*, 2025, **16**, 3142.

[S13] J. Heo, D. Dong, Z. Wang, F. Chen and C. Wang, *Joule*, 2025, **9**, 101844.

[S14] J. Cong, Y. Wang, X. Lin, Z. Huang, H. Wang, J. Li, L. Hu, H. Hua, J. Huang and Y.-C. Lin, *J. Am. Chem. Soc.*, 2025, **147**, 8607-8617.

[S15] S. Han, M. Li, Q. Fan, Z. Han, X. Ming, W. Wang, W. Cai and H. Niu, *Energy Environ. Sci.*, 2025, **18**, 4186-4199.

[S16] Y. Li, L. Liu, H. Zhang, H. Wang, Z. Sun, Z. Zhang, W. Pang, S. Omanovic, S. Sun and X. Chen, *Adv. Funct. Mater.*, 2025, **35**, 2410855.

[S17] H. Lin, L. Zeng, C. Lin, J. Wu, H. He, C. Huang, W. Lai, P. Xiong, F. Xiao and Q. Qian, *Energy Environ. Sci.*, 2025, **18**, 1282-1293.

[S18] K. Guan, W. Chen, Y. Yang, F. Ye, Y. Hong, J. Zhang, Q. Gu, Y. Wu and L. Hu, *Adv. Mater.*, 2024, **36**, 2405889.

[S19] J. Bu, P. Liu, G. Ou, M. Ye, Z. Wen, Y. Zhang, Y. Tang, X. Liu and C. C. Li, *Adv. Mater.*, 2025, **37**, 2420221.

[S20] K. Liu, M. Sun, Y. Wu, T. Zhang, A. Zhu, S. Bu, C. Luan, K. Liu, Y. Zhou and D. Lin, *Adv. Mater.*, 2025, **37**, 2420079.

[S21] Q. Kang, H. Liang, Z. Zhu, F. Xing, B. Zhu, Y. Li, S. Wang, S. Tang, H. Li and L. Pan, *Angew. Chem. Int. Ed.*, 2025, **64**, e202420183.

[S22] H. Ren, S. Li, L. Xu, L. Wang, X. Liu, L. Wang, Y. Liu, L. Zhang, H. Zhang and Y. Gong, *Angew. Chem. Int. Ed.*, 2025, **137**, e202423302.

[S23] Z. Peng, L. Tang, S. Li, L. Tan and Y. Chen, *Angew. Chem. Int. Ed.*, 2025, **64**, e202418242.

[S24] D. Xu, X. Ren, H. Li, Y. Zhou, S. Chai, Y. Chen, H. Li, L. Bai, Z. Chang and A. Pan, *Angew. Chem. Int. Ed.*, 2024, **136**, e202402833.

[S25] S. Li, X. Chen, J. Zhao, Y. Zhang, K. Zhang, K. Wang, J. Shen, P. Lv, Y. Jia and Y. Bai, *ACS Energy Lett.*, 2025, **10**, 1642-1653.

[S26] B. Hu, T. Chen, Y. Wang, X. Qian, Q. Zhang and J. Fu, *Adv. Energy Mater.*, 2024, **14**, 2401

